Acta Pharmaceutica Sinica B xxxx;xxx(xxx):xxx

Chinese Pharmaceutical Association
Institute of Materia Medica, Chinese Academy of Medical Sciences

Acta Pharmaceutica Sinica B

www.elsevier.com/locate/apsb
www.sciencedirect.com

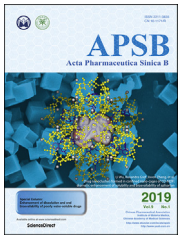

ORIGINAL ARTICLE

Gas-propelled nanomotors alleviate colitis through the regulation of intestinal immunoenvironment-hematopexis-microbiota circuits

Bo Xiao[a,b,*], Yuqi Liang[b,*], Ga Liu[b], Lingshuang Wang[b], Zhan Zhang[c,d], Libin Qiu[b], Haiting Xu[b], Sean Carr[d,e], Xiaoxiao Shi[b], Rui L. Reis[f], Subhas C. Kundu[f], Zhenghua Zhu[a,*]

[a]*Department of Gastroenterology, The First Affiliated Hospital of Nanchang University, Nanchang 330006, China*
[b]*College of Sericulture, Textile, and Biomass Sciences, Southwest University, Chongqing 400715, China*
[c]*Department of Neurology, School of Medicine, Emory University, Atlanta, GA 30322, USA*
[d]*Atlanta Veterans Affairs Medical Center, Decatur, GA 30033, USA*
[e]*Department of Surgery, School of Medicine, Emory University, Atlanta, GA 30322, USA*
[f]*3Bs Research Group, I3Bs — Research Institute on Biomaterials, Biodegradables and Biomimetics, University of Minho, Headquarters of the European Institute of Excellence on Tissue Engineering and Regenerative Medicine, AvePark, Barco, Guimaraes 4805-017, Portugal*

Received 28 September 2023; received in revised form 5 December 2023; accepted 18 December 2023

KEY WORDS

Nanomotor;
Anti-inflammation;
Blood coagulation;
Immune regulation;
Hematopexis;
Microbiota rebalance;
Ulcerative colitis;
Rectal administration

Abstract The progression of ulcerative colitis (UC) is associated with immunologic derangement, intestinal hemorrhage, and microbiota imbalance. While traditional medications mainly focus on mitigating inflammation, it remains challenging to address multiple symptoms. Here, a versatile gas-propelled nanomotor was constructed by mild fusion of post-ultrasonic CaO_2 nanospheres with Cu_2O nanoblocks. The resulting CaO_2−Cu_2O possessed a desirable diameter (291.3 nm) and a uniform size distribution. It could be efficiently internalized by colonic epithelial cells and macrophages, scavenge intracellular reactive oxygen/nitrogen species, and alleviate immune reactions by pro-polarizing macrophages to the anti-inflammatory M2 phenotype. This nanomotor was found to penetrate through the mucus barrier and accumulate in the colitis mucosa due to the driving force of the generated oxygen bubbles. Rectal administration of CaO_2−Cu_2O could stanch the bleeding, repair the disrupted colonic epithelial layer, and reduce the inflammatory responses through its interaction with the genes relevant to blood

*Corresponding authors.
E-mail addresses: bxiao@swu.edu.cn (Bo Xiao), yq.liang.work@foxmail.com (Yuqi Liang), zhuzhenhua19820122@163.com (Zhenghua Zhu).
Peer review under the responsibility of Chinese Pharmaceutical Association and Institute of Materia Medica, Chinese Academy of Medical Sciences.

https://doi.org/10.1016/j.apsb.2024.02.008

Please cite this article as: Xiao Bo et al., Gas-propelled nanomotors alleviate colitis through the regulation of intestinal immunoenvironment-hematopexis-microbiota circuits, Acta Pharmaceutica Sinica B, https://doi.org/10.1016/j.apsb.2024.02.008

coagulation, anti-oxidation, wound healing, and anti-inflammation. Impressively, it restored intestinal microbiota balance by elevating the proportions of beneficial bacteria (*e.g.*, *Odoribacter* and *Bifidobacterium*) and decreasing the abundances of harmful bacteria (*e.g.*, *Prevotellaceae* and *Helicobacter*). Our gas-driven CaO_2−Cu_2O offers a promising therapeutic platform for robust treatment of UC *via* the rectal route.

1. Introduction

Ulcerative colitis (UC) is a chronic and recurrent inflammatory disorder in the colon, whose incidence has increased significantly in recent years[1,2]. As the largest immune organ, the colon overprotects itself from antigens when continuously exposed to intestinal contents, thereby causing intestinal inflammation[3]. Although the pathogenesis of UC remains unknown, the severe rectal bleeding, excessive reactive oxygen/nitrogen species (ROS/RNS), over-expression of pro-inflammatory cytokines (*e.g.*, TNF-α, IL-6, and IL-12), and activation of immune cells are strongly associated with the occurrence and progression of UC[4-6]. The intestinal microbiota is crucial for the immune homeostasis of the gastrointestinal tract (GIT), and its most striking characteristics are abundance and diversity[7]. However, intestinal microbiota balance is disturbed in UC patients and UC mouse models[8,9]. In practice, conventional therapeutic strategies aim to alleviate pro-inflammatory reactions[10]. For instance, current first-line treatments for UC mainly include oral, rectal, and intravenous administrations of 5-aminosalicylic acid, corticosteroids, and immunosuppressants, which have multiple disadvantageous restrictions, such as unsatisfactory therapeutic outcomes and severe side effects[11]. Although oral administration is a preferable route for drug delivery to the diseased gastrointestinal tissues, the massive drug degradation in the digestive juice and the viscous mucus barrier greatly diminish drug bioavailability[12,13]. Thus, the synergistic choices of the effective therapeutic system and the administration route are indispensable to improving the therapeutic effect of UC.

Previously, to overcome the mucus barrier, nanoparticles (NPs) were coated with mucus-inert polymers (*e.g.*, polyethylene glycol, lipid, Pluronic F127, and fluorinated polymer)[14-17]. Unfortunately, the high molecular weights of these polymers and the chain entanglement effect largely impair the mucus-penetrating performance of NPs. Recently, the locomotor activities of NPs were enhanced by external physical stimuli (*e.g.*, ultrasound, near-infrared, and magnetic field) to overcome the movement barriers[18]. However, this strategy is limited by multiple external factors (*e.g.*, accurate penetration, processing time, and guidance). By contrast, autonomous self-propelling NPs by gas (*e.g.*, NO, O_2, and CO_2) reveal the preponderance of quickly generated gas bubbles and the independence of external driving forces[19-21]. Among the gas-generating materials, calcium peroxide (CaO_2) NPs emit their charm on oxygen generation and Ca^{2+}-dependent therapeutic functions[22]. It is reported that Ca^{2+}, a metal coagulation factor IV, securely activates the thrombin pathway by promoting the conversion of fibrinogen and platelet activation[23,24]. Copper (Cu) is a key microelement, which plays crucial roles in modulating the immune system, redox balance, and tissue regeneration[25]. Therefore, the combination of CaO_2 and Cu is speculated to overcome the delivery barriers and achieve synergistic therapeutic effects against UC after rectal administration.

In the present study, we constructed a versatile gas-propelled nanomotor (CaO_2−Cu_2O) with enhanced mucus penetration and colitis mucosa accumulation properties. This NP played a prominent part in ROS/RNS scavenging, down-regulation of pro-inflammatory factors, precaution of tissue damage, and blood coagulation, as shown in Scheme 1. Rectal therapies offer a number of advantages, including direct drug delivery to inflammatory sites in the distal colon, rapid response of patients to therapeutics, and reduced systemic drug exposure[26,27]. Upon rectal administration, CaO_2−Cu_2O could self-impulsively penetrate through the mucous layer due to oxygen generation following accumulating into the colitis tissues. The *in vitro* and *in vivo* experiments verified their ability to repair mucosa barriers and restore colon lengths, body weights, and pro-inflammatory cytokines to healthy levels, illustrating their efficient preventive and therapeutic results. Finally, the therapeutic mechanisms of CaO_2−Cu_2O, including immune regulation, wound healing, and flora modulation, were detected by transcriptomics and 16S ribosomal RNA (rRNA) sequencing.

2. Materials and methods

2.1. Preparation of CaO_2, Cu_2O, and CaO_2−Cu_2O

Briefly, cupric chloride ($CuCl_2$) solution (10 mmol/L, 15 mL) was heated to 80 °C for 10 min by an oil bath heating method, and ascorbic acid solution (100 mmol/L, 50 mL) was dropped into the above solution for a 12-h redox reaction. After that, Cu_2O NPs were collected through centrifugation at 7000×*g*. After freeze-drying, Cu_2O was dispersed in ethanol. The preparation of CaO_2 was as follows: calcium chloride ($CaCl_2$, 300 mg), polyethylene glycol 200 (PEG-200, 12 mL), and ammonium hydroxide (2.5 mL) were dissolved in deionized water (3 mL), and hydrogen peroxide (H_2O_2) solution (1.5 mL) was dropped into the mixture. After a 4-h reaction, the sodium hydroxide solution was dropped to adjust the pH value to 11.5. CaO_2 NPs were collected through centrifugation at 7000×*g* (Hitachi, CP100NX, Tokyo, Japan) and dispersed in ethanol. The obtained CaO_2 suspension was sonicated for 10 min at an amplitude of 30%, while Cu_2O suspension was sonicated for 10 min at 150 W using a Sonifier 450 (Branson Sonic Power, Danbury, CT, USA). These two suspensions were mixed and stirred for 4 h at 80 °C. The resultant CaO_2−Cu_2O was collected through centrifugation at 7000×*g* and obtained by a rotary evaporator.

Please cite this article as: Xiao Bo et al., Gas-propelled nanomotors alleviate colitis through the regulation of intestinal immunoenvironment-hematopexis-microbiota circuits, Acta Pharmaceutica Sinica B, https://doi.org/10.1016/j.apsb.2024.02.008

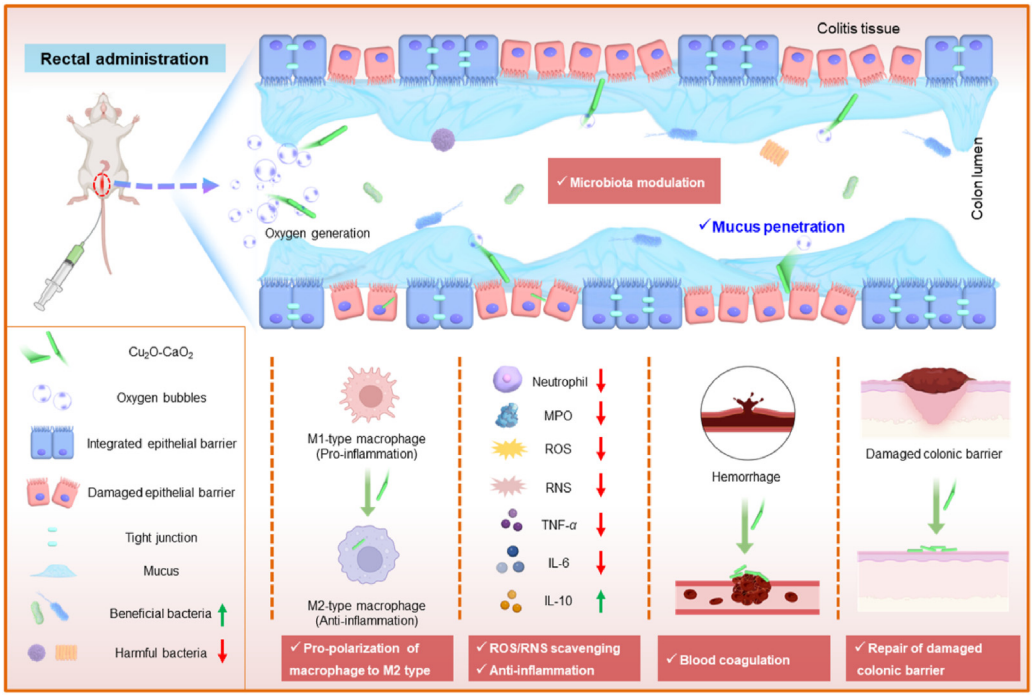

Scheme 1 Schematic diagram of CaO_2−Cu_2O as gas-driven nanomotors for effective treatment of UC through mucus penetration, colitis mucosa accumulation, ROS/RNS scavenging, down-regulation of inflammatory reaction, blood coagulation, wound healing, and intestinal microbiota modulation after rectal administration.

2.2. *Oxygen-generating property of NPs*

CaO_2 and CaO_2−Cu_2O (10 mg) were added into sample bottles with stimulated colonic fluid (SCF). The oxygen-generating progress was recorded with a camera every 30 s for 3 min. To investigate the real-time oxygen releasing profiles of CaO_2−Cu_2O, the concentrations of oxygen in SCF were measured by a dissolved oxygen meter (Shanghai INESA Scientific Instrument Co., Ltd., JPBJ-608, Shanghai, China). The instrument sensor probe was put into zero-oxygen water for zero calibration, and the detected probe was dipped into SCF with a constant stir at room temperature. When the display count stabilized, CaO_2 and CaO_2−Cu_2O (10 mg) were added to the solutions at a final concentration of 1 mg/mL. The portable dissolved oxygen meter was applied to record the dissolved oxygen concentrations during the first 3 min.

2.3. *In vitro anti-inflammatory activity of NPs*

Raw 264.7 macrophages were seeded in 24-well plates at a final density of 1×10^5 cells per well. After overnight culture, cells were incubated with CaO_2 and CaO_2−Cu_2O at a final Cu concentration of 100, 200, 400, and 800 ng/mL for 24 h and rinsed with cold PBS. Lipopolysaccharide (LPS, 0.5 μg/mL, 300 μL) was added to the wells of the positive control and experimental groups. After 3-h incubation, the supernatant was collected after centrifugation at 1000*g* for 15 min, and the concentrations of TNF-α, IL-6, and IL-10 were measured by their corresponding enzyme-linked immunosorbent assay (ELISA) kits (Solarbio, Shanghai, China). Raw 264.7 macrophages without the treatment of LPS were treated as a negative control, whereas LPS-stimulated cells (without NP treatment) were treated as a positive control.

2.4. *Mucus penetrating capacity of NPs*

Hydroxyethyl cellulose (HEC, 1%, *w*/*v*; 200 μL) was added to the Petri dish to simulate the colonic mucus. Subsequently, coumarin (Cou)-labeled CaO_2 (CaO_2@Cou) and Cou-labeled CaO_2−Cu_2O (CaO_2−Cu_2O@Cou) suspensions (50 μL) were added to the surface of the simulated mucus, and the penetration profiles of NPs were recorded by confocal laser scanning microscopy (CLSM, Olympus Corporation, FV3000, Tokyo, Japan).

2.5. *In vivo therapeutic outcomes of CaO_2−Cu_2O against UC*

All animal protocols were approved by the Southwest University Institutional Animal Care and Use Committee (IACUC-20210610-02). Female Kunming and C57/BL6 mice (8 weeks) were purchased from Ensiweier Biotechnology Co., Ltd. (Chongqing, China). The UC mouse model was established by supplying mice with dextran sulfate sodium (DSS, 3.5%, *w*/*v*)-contained drinking water. Mice were treated with DSS (3.5%, *w*/*v*) for 4 days. Once the UC mouse model was established, all drinking water was replaced with deionized water on Day 5. Mice were fasted for 12 h (Days 5, 8, 11, 14, and 17) before the treatment of CaO_2 and CaO_2−Cu_2O suspensions (2 mg/kg, 150 μL). In contrast, the DSS control and healthy control groups were given equal doses of saline. The anus photos, mouse body weights, and DAI values of all the groups were observed and recorded at scheduled time points. Mice were sacrificed on Day 21, and the isolated colons were weighed and collected for hematoxylin-eosin (H&E), periodic acid-Schiff (PAS), and immunofluorescence staining. The concentrations of various cytokines (TNF-α, IL-6, and IL-10) in the serum were quantified by their corresponding ELISA kits (Solarbio, Shanghai, China).

Please cite this article as: Xiao Bo et al., Gas-propelled nanomotors alleviate colitis through the regulation of intestinal immunoenvironment-hematopexis-microbiota circuits, Acta Pharmaceutica Sinica B, https://doi.org/10.1016/j.apsb.2024.02.008

2.6. Statistical analysis

Statistical analysis was conducted using a Student's *t*-test or ANOVA test, followed by a Bonferroni *post-hoc* test (GraphPad Prism). Data were presented as mean ± standard error of the mean (SEM). Statistical significance was expressed by $^{*}P < 0.05$, $^{**}P < 0.01$, and $^{***}P < 0.001$.

3. Results and discussion

3.1. Preparation and physicochemical characterization of CaO_2−Cu_2O

The fabrication process of CaO_2−Cu_2O is illustrated in Fig. 1A. As revealed by scanning electron microscopy (SEM), CaO_2−Cu_2O possessed a crystalline rod shape and a uniform particle size of 305.1 nm in length and 121.6 nm in diameter (Fig. 1B). Dynamic light scattering (DLS) demonstrated that CaO_2−Cu_2O with a uniform distribution had a mean hydrodynamic particle size of ∼291.3 nm (Fig. 1C). In contrast, sphere-like CaO_2 and block-shaped Cu_2O exhibited much smaller hydrodynamic sizes of ∼159.1 and ∼135.4 nm, respectively (Supporting Information Fig. S1). Element maps showed the distribution profiles of Ca, Cu, and O in CaO_2−Cu_2O, which could be deemed as proof of the successful fabrication of CaO_2−Cu_2O (Fig. 1D and Supporting Information Fig. S2A). The weak energy dispersive spectroscopy (EDS) signal of the Cu element might be ascribed to the resolution limitation of the SEM instrument. To confirm the existence of the Cu element, we prepared CaO_2−Cu_2O powders and determined the Cu element again. It is clear to observe the presence of Cu element in CaO_2−Cu_2O (Fig. S2B). Moreover, compositions and chemical states of the elements determined by X-ray photoelectron spectroscopy (XPS) further chemically affirmed the successful acquisition of CaO_2−Cu_2O, of which the characteristic signal peaks at 953.0 and 932.8 eV corresponded to the binding energy of $Cu2p_{1/2}$ and $Cu2p_{3/2}$, respectively (Fig. 1E and Fig. S2C). The loading contents of Ca and Cu in CaO_2−Cu_2O were quantified as 47.1 and 26.7% (*w*/*w*) by inductively coupled plasma (ICP), respectively (Supporting Information Fig. S3).

During the progression of inflammatory diseases, reactive species are excessively produced, which induce irreversible oxidative damage to the cellular components, such as lipids, proteins, and nucleic acids[28]. Thus, free radical scavenging is vital for the treatment of inflammatory diseases. Initially, we demonstrated the ROS scavenging ability of CaO_2−Cu_2O by 2,2′-azinobis(3-ethylbenzothiazoline-6-sulfonic acid) diammonium salt (ABTS) kit. As shown in Fig. 1F, CaO_2 exhibited no anti-oxidative effect, while CaO_2−Cu_2O presented an obvious anti-oxidative capacity in a concentration-dependent manner. Thereafter, we evaluated the elimination efficiencies of H_2O_2 and $O_2^{\bullet-}$ by CaO_2−Cu_2O and their superoxide dismutase (SOD)-like nanoenzyme performance. It was observed that CaO_2−Cu_2O showed strong H_2O_2 and $O_2^{\bullet-}$ scavenging activities with a positive correlation between their concentrations and anti-oxidative activities (Fig. 1G and H). In particular, at a Cu concentration of 250 ng/mL, the inhibition rates of H_2O_2 and $O_2^{\bullet-}$ activities reached approximately 60.7% and 50.8%, respectively. SOD, as an anti-oxidase, is a principal enzyme responsible for scavenging free radicals[29], which could be utilized as a marker to estimate the anti-oxidative ability of CaO_2−Cu_2O. Fig. 1I reveals the SOD-mimic activity of CaO_2−Cu_2O, which showed an upward trend with increasing Cu concentrations. Notably, the SOD activity of CaO_2−Cu_2O approached 90.0% when Cu concentrations reached 1000 ng/mL. The excellent radical scavenging and SOD-mimic activities of CaO_2−Cu_2O lay the foundation for eliminating reactive species in the inflammatory tissues.

3.2. In vitro biocompatibility, anti-inflammation, and anti-oxidation of CaO_2−Cu_2O

The biocompatibility of nanotherapeutics is critical for their biomedical applications[30]. Therefore, the viability of cells receiving the treatment of CaO_2−Cu_2O was examined by the methyl tetrazolium (MTT) assay. After co-incubation for 24 and 48 h, the viabilities of CT-26 cells and Raw 264.7 macrophages with the treatment of CaO_2 significantly decreased (below 61.0%), starting from 2 μg/mL (Supporting Information Fig. S4). This observation might be attributed to the fact that CaO_2 triggers the instantaneous overload of intracellular Ca^{2+}, thereby inducing cellular apoptosis[31]. It is worth noting that the introduction of Cu_2O to the nanomotors significantly increased their viabilities, indicating that introducing Cu_2O could improve the biocompatibility of CaO_2−Cu_2O. Consistently, few dead cells were observed, and over 90.0% of cells were live after the treatment of CaO_2−Cu_2O for 24 h (Supporting Information Fig. S5). In addition, unprevailing cell growth was detected in the cell migration experiment (Supporting Information Fig. S6), confirming the good *in vitro* biocompatibility of CaO_2−Cu_2O.

Macrophage has an integral function in the immune regulation of UC[32]. Based on this, the time-dependent internalization profiles of CaO_2@Cou and CaO_2−Cu_2O@Cou by Raw 264.7 macrophages were determined by flow cytometry (FCM) (Supporting Information Fig. S7A−S7C). The encapsulation efficiencies of Cou in CaO_2−Cu_2O@Cou and Cu_2O@Cou were 5.8% and 7.6%, respectively, which were detected using a fluorescence spectrophotometer. Three hours after co-incubation, the internalization percentage of the CaO_2−Cu_2O@Cou-treated macrophages surpassed 90%, and no significant difference in cellular uptake efficiencies was observed between CaO_2@Cou and CaO_2−Cu_2O@Cou. CLSM further revealed that CaO_2−Cu_2O@Cou (green fluorescence) was internalized and distributed within macrophages after 2-h incubation (Fig. S7D), demonstrating the preferential internalization of CaO_2−Cu_2O by macrophages. The progression of inflammatory diseases leads to the infiltration of immune cells into the inflamed tissues. These cells secret abundant pro-inflammatory cytokines (*e.g.*, TNF-α and IL-6), which exacerbate inflammatory responses and accelerate tissue damage[33]. As presented in Fig. 2A−C, TNF-α and IL-6 were remarkably elevated when macrophages were exposed to the main cytoderm components of Gram-negative bacteria, LPS. Interestingly, the secreted levels of TNF-α and IL-6 in the CaO_2−Cu_2O-treated group markedly decreased in a concentration-dependent manner, suggesting that CaO_2−Cu_2O could effectively block LPS-induced inflammation and had the potential to nullify the cytokine storm. Conversely, the treatment of CaO_2−Cu_2O significantly increased the levels of IL-10 (a typical anti-inflammatory cytokine) when compared with the positive control (Fig. 2D). Relative to the weak anti-inflammatory activity of CaO_2, the strong capacity of CaO_2−Cu_2O to down-regulate the levels of pro-inflammatory cytokines demonstrate the beneficial functions of copper ions in the treatment of inflammatory diseases, which is consistent with previous studies[25,34].

Please cite this article as: Xiao Bo et al., Gas-propelled nanomotors alleviate colitis through the regulation of intestinal immunoenvironment-hematopexis-microbiota circuits, Acta Pharmaceutica Sinica B, https://doi.org/10.1016/j.apsb.2024.02.008

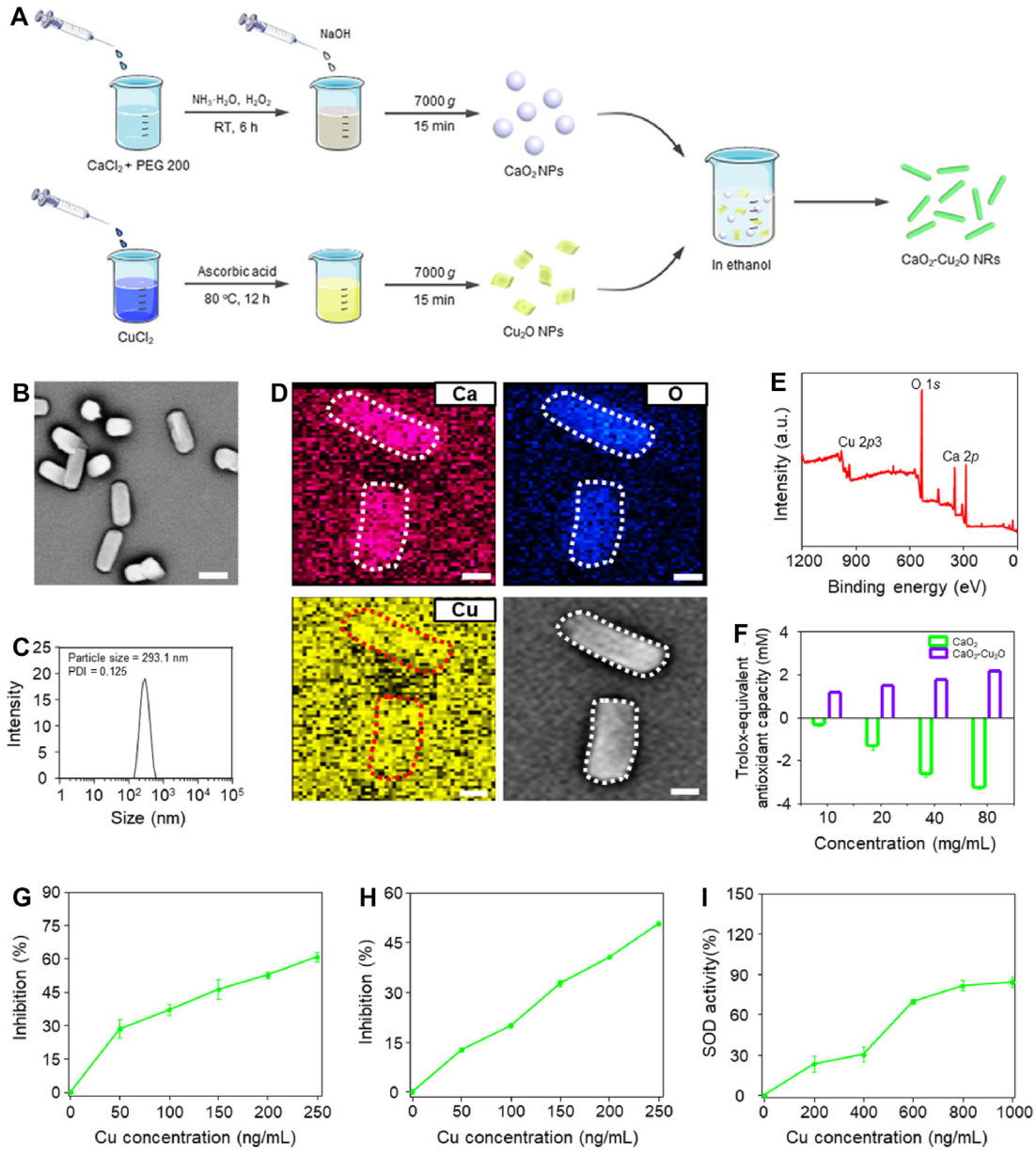

Figure 1 Fabrication and physicochemical characterization of CaO_2−Cu_2O. (A) Schematic diagram of the synthetic processes of CaO_2−Cu_2O. (B) SEM image and (C) hydrodynamic size distribution of CaO_2−Cu_2O. The scale bar represents 200 nm. (D) Distribution of elements in CaO_2−Cu_2O, which were examined by EDS analysis. The scale bar represents 100 nm. (E) The whole spectrum of CaO_2−Cu_2O by XPS analysis. (F) Trolox-equivalent anti-oxidative capacity of CaO_2 and CaO_2−Cu_2O with different NP concentrations (10, 20, 40, and 80 mg/mL). (G) H_2O_2 and (H) $O_2^{\bullet-}$ scavenging capacities of CaO_2−Cu_2O with different Cu concentrations (50, 100, 150, 200, and 250 ng/mL). (I) SOD-like activity of CaO_2−Cu_2O with different Cu concentrations (200, 400, 600, 800, and 1000 ng/mL). Data are expressed as means ± SEM (n = 3).

ROS and RNS play a critical role in the inflammatory process, which influence the adjustment of physiological activators[35]. Inspired by the reactive species scavenging capacity of CaO_2−Cu_2O at the material level, we benchmarked their ability to eliminate intracellular ROS and RNS by using 2',7'-dichlorofluorescein diacetate (DCFH-DA) and 4-amino,5-aminomethyl-2',7'-difluorescein diacetate (DAF-FM-DA) fluorescence probes, respectively. CLSM images (Fig. 2E) and the corresponding quantitative results (Fig. 2F) displayed a contrasting result that bright green fluorescence signals (ROS) were present in the positive control cells and the CaO_2-treated cells. In contrast, the CaO_2−Cu_2O-treated cells showed negligible green signals, which confirmed the excellent intracellular ROS scavenging capability of CaO_2−Cu_2O. Fig. 2G and H further illustrated that CaO_2−Cu_2O exhibited much better RNS scavenging capacity than CaO_2. The FCM data (Fig. 2I−N) was in good agreement with the CLSM images, in which CaO_2−Cu_2O possessed improved ROS/RNS scavenging activities according to the lower fluorescence intensity histogram, compared with CaO_2.

Please cite this article as: Xiao Bo et al., Gas-propelled nanomotors alleviate colitis through the regulation of intestinal immunoenvironment-hematopexis-microbiota circuits, Acta Pharmaceutica Sinica B, https://doi.org/10.1016/j.apsb.2024.02.008

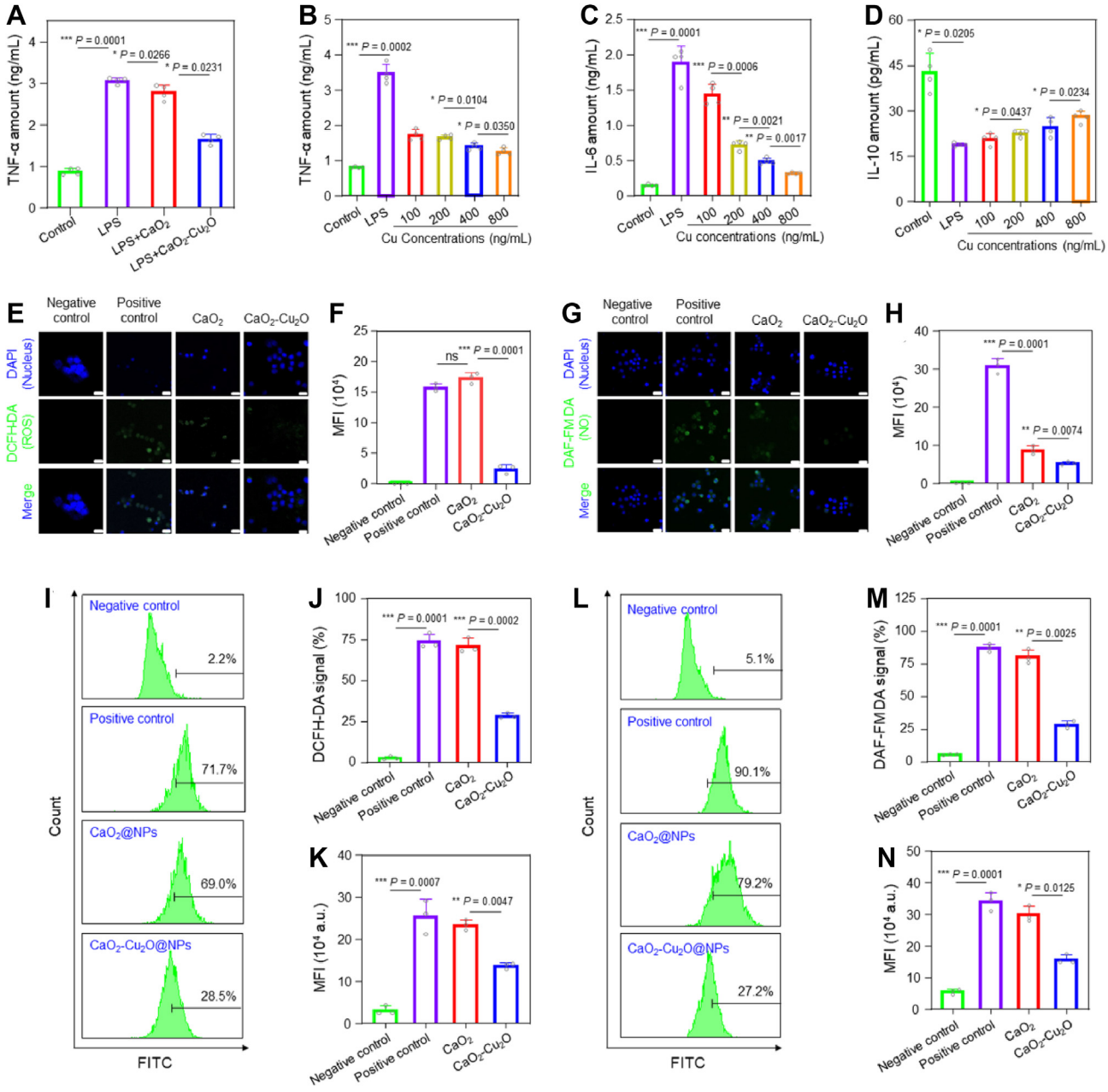

Figure 2 *In vitro* anti-inflammatory and anti-oxidative activities of CaO_2−Cu_2O. (A) The secreted amounts of TNF-α from Raw 264.7 macrophages receiving the treatment of CaO_2 and CaO_2−Cu_2O at an equal NP concentration. The secreted amounts of (B) TNF-α, (C) IL-6, and (D) IL-12 from Raw 264.7 macrophages with the treatment of CaO_2−Cu_2O at different Cu concentrations (100, 200, 400, and 800 ng/mL). Raw 264.7 macrophages without LPS stimulation were treated as a negative control, whereas LPS (1.0 μg/mL)-stimulated Raw 264.7 macrophages were treated as a positive control. Fluorescence images and mean fluorescence intensities of intracellular (E, F) ROS and (G, H) RNS in Raw 264.7 macrophages were detected by two fluorescence probes (DCFH-DA and DAF-FM-DA) after treatment with various NPs. The scale bar represents 20 μm. Flow cytometric histograms of the fluorescence intensities and the corresponding quantitative results of intracellular (I−K) ROS or (L−N) RNS after treatment with various NPs. Data are expressed as means ± SEM ($n = 3$; $^*P < 0.05$, $^{**}P < 0.01$, and $^{***}P < 0.001$).

3.3. *Hemostatic activity, mucus penetration, and colonic accumulation of CaO_2−Cu_2O*

Hematochezia is typically observed in UC patients, which is a life-threatening indicator induced by leaky intestinal vessels and impaired colonic mucosa[36,37]. Thus, hemostasis has been raised as a primary therapeutic aim for UC treatment[38]. Here, the severed tail model of Kunming mice was used to predict the prospect of CaO_2−Cu_2O in stanching bleeding. Fig. 3A and B indicate that CaO_2−Cu_2O showed rapid homeostatic performance within 30 s,

Please cite this article as: Xiao Bo et al., Gas-propelled nanomotors alleviate colitis through the regulation of intestinal immunoenvironment-hematopexis-microbiota circuits, Acta Pharmaceutica Sinica B, https://doi.org/10.1016/j.apsb.2024.02.008

whereas CaO_2 treatment exacerbated postoperative bleeding. These observations might be ascribed to the fact that CaO_2 has stronger oxygen-generating capacity than CaO_2−Cu_2O, and the burst generation of large amounts of oxygen bubbles by CaO_2 can dilate blood vessels, resulting in the acceleration of hemorrhage. We further found that the CaO_2−Cu_2O-treated group had the least amount of blood loss (Fig. 3C) and the shortest hemostasis time (Fig. 3D). Moreover, the hemostatic effect of CaO_2−Cu_2O was confirmed in the DSS-induced colonic bleeding mice. It was observed that the treatment of CaO_2−Cu_2O obviously relieved the colonic bleeding phenomenon (Supporting Information Fig. S8A) and decreased the gastrointestinal bleeding values (Fig. S8B) compared with the DSS control group. These observations suggest that CaO_2−Cu_2O possesses the potential to prevent UC-associated colonic bleeding.

The mucus remains the main obstacle, limiting nanomedicines from reaching the inflamed areas of the colonic mucosa[39]. Self-propelled nanomotors, *via* the generation of impetus (*e.g.*, CO_2, H_2, and O_2), provide a promising therapeutic platform for promoting deep tissue penetration[40]. The schematic illustration (Fig. 3E) represents that the CaO_2 component can drive nanomotors (CaO_2−Cu_2O) to the colitis tissues *via* the persistent and steady generation of oxygen bubbles. When CaO_2 and CaO_2−Cu_2O reacted with SCF, they were gradually disrupted and produced large amounts of bubbles (Supporting Information Videos S1 and S2). Quantitatively, their oxygen-generating capabilities were time-dependent, and the accumulative concentration of the generated oxygen reached approximately 11 mg/L after incubation for 3 min (Fig. 3F). Next, the motion performance of CaO_2−Cu_2O was evaluated in the colonic mucus-like hydrogels (pH 6.5 and pH 5.5). HEC hydrogel possesses microrheology similar to colonic mucus, and thus, it has been used as a mucus-simulating gel[41]. It can be seen in Supporting Information Figs. S9A−S9C that after incubation in the mucus-like hydrogels for 5 s, CaO_2−Cu_2O moved to large ranges, which were even larger than that of H_2O_2 and ultrasound dual-driven nanomotors in our previous study[39]. The locomotor activity of CaO_2−Cu_2O was significantly improved when presented in the hydrogel (pH 5.5), resulting in enhanced diffusion capacity. Notably, the pH value of the reaction solution was only slightly changed (less than 0.6) at the end of the chemical reaction (Fig. S9D), suggesting that the reaction could not greatly destabilize the acidity of the colonic microenvironment.

Supporting video related to this article can be found at https://doi.org/10.1016/j.apsb.2024.02.008

To show direct evidence that CaO_2−Cu_2O has an improved mucus penetrating capacity, we comparatively determined the mucus penetrating profiles of CaO_2 and CaO_2−Cu_2O in the HEC hydrogel. As revealed in Fig. 3G, CaO_2−Cu_2O@Cou achieved a more profound penetration distance (∼100 μm) than its counterpart (Cu_2O@Cou) after 30 min of incubation. Moreover, the generated oxygen bubbles significantly improved the unidirectional movement and wide distribution of CaO_2−Cu_2O (Supporting Information Fig. S10), providing a substantial foundation for its enhanced mucus penetration and subsequent colitis mucosa accumulation. Subsequently, we encapsulated the fluorescence probe (Cou) into the NPs to track their distribution after rectal administration. It can be seen in Fig. 3H that the fluorescence intensities of all the colons gradually decreased, and the colons from the CaO_2−Cu_2O@Cou-treated mice showed stronger fluorescence signals than those from the Cu_2O@Cou-treated mice at different time points (1, 2, 6, and 12 h). The fluorescence staining of colon tissue sections confirmed the presence of NPs (Cu_2O@Cou and CaO_2−Cu_2O@Cou) in the colonic mucosa, except that much brighter green fluorescence was detected from the CaO_2−Cu_2O@Cou-treated group compared with the group receiving the treatment of Cu_2O@Cou (Fig. 3I). Furthermore, we quantified the contents of Ca and Cu in the colitis tissues after rectal administration of different samples. It was detected that the contents of Ca and Cu in the colitis tissues from the CaO_2−Cu_2O-treated group were much more than those from the groups receiving rectal administration of Cu_2O and CaO_2 (Supporting Information Fig. S11), which might be attributed to the strongest penetration capacity of CaO_2−Cu_2O. These results collectively demonstrate that the introduction of CaO_2 endows CaO_2−Cu_2O with strong *in vivo* mucus penetration and mucosa accumulation capacities. As reported, drugs are required to be delivered to the target sites to exert their therapeutic effect[42,43]. Considering the very small amount of Cu_2O accumulated in the colitis tissues (Fig. 3G and I), Cu_2O was not set as a control in the subsequent experiments.

3.4. *In vivo preventive effect of CaO_2−Cu_2O against UC*

To examine the therapeutic effect of CaO_2−Cu_2O against UC, we administrated these NPs to the DSS-induced UC mouse model *via* the rectal route. The experimental design was shown in Fig. 4A. It was observed that the DSS control group showed apparent body weight loss (12.0%) and increased disease activity indexes (DAIs) on Day 9. Rectal administration of CaO_2 had no retardation effect on weight loss and DAI increase. At the same time, CaO_2−Cu_2O treatment successfully prevented mice from weight loss (Fig. 4B) and increased DAI (Fig. 4C). The CaO_2−Cu_2O-treated group possessed comparable colon lengths to the healthy group. On the contrary, the DSS control and CaO_2-treated groups had relatively short colon lengths (Fig. 4D). Increased spleen weight and elevated myeloperoxidase (MPO) activities reflect the severity of colonic inflammation due to the proliferation of macrophages and neutrophils and their infiltration into the inflammatory sites[44]. CaO_2−Cu_2O elicited protection against spleen weight gain (Fig. 4E) and an effective reduction in the colonic MPO activity (Fig. 4F) relative to the levels of the DSS control group and the CaO_2-treated group.

We further verified whether CaO_2−Cu_2O could potentially shift the expression profiles of pro- and anti-inflammatory cytokines in the DSS-treated mice. Upon establishment of UC, the amounts of pro-inflammatory cytokines (*e.g.*, TNF-α and IL-6) were found to be increased, which were accompanied by the reduced levels of anti-inflammatory cytokine (*e.g.*, IL-10) (Fig. 4G−I). Notably, CaO_2−Cu_2O skewed the cytokine milieu towards an anti-inflammatory state. It was detected that rectal administration of CaO_2−Cu_2O from Day two to Day 8, every three days, successfully reversed the expression levels of pro-inflammatory cytokines and largely restored the secretion of anti-inflammatory IL-10 to the healthy control level. However, CaO_2 alone had a diminished effect on reversing the expression levels of DSS-induced pro- and anti-inflammatory cytokines.

Subsequently, H&E and PAS staining were performed to examine the inflammation severities and mucus amounts.

Please cite this article as: Xiao Bo et al., Gas-propelled nanomotors alleviate colitis through the regulation of intestinal immunoenvironment-hematopexis-microbiota circuits, Acta Pharmaceutica Sinica B, https://doi.org/10.1016/j.apsb.2024.02.008

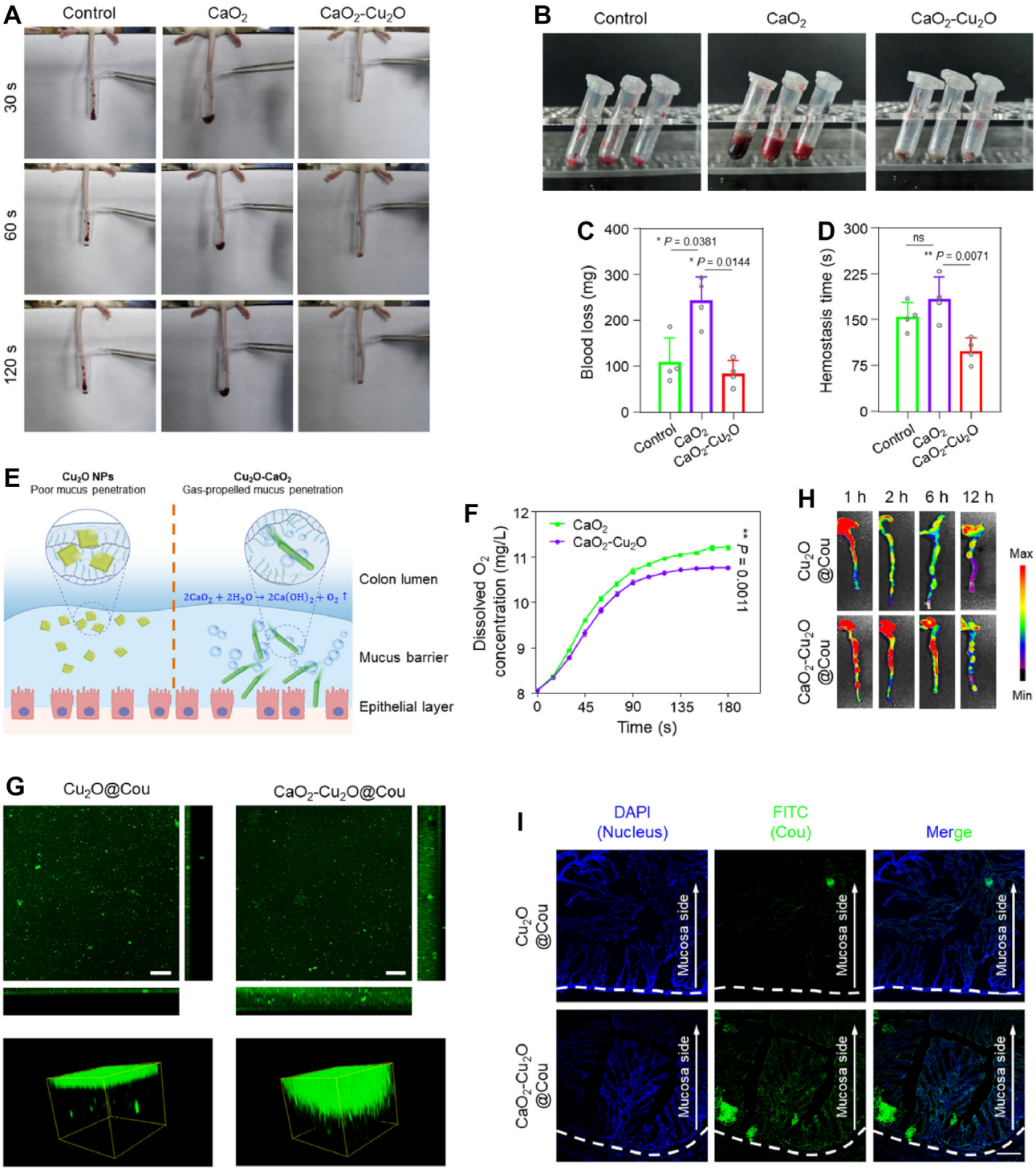

Figure 3 Hemostatic activity, mucus penetration, and colonic accumulation of CaO_2−Cu_2O. (A) Images of the hemorrhage symptom in the tail cutting test after treatment with different NPs for 30, 60, and 120 s, respectively. (B) Images of blood collecting tubes from mice receiving the treatment of CaO_2 and CaO_2−Cu_2O. (C) Blood loss amounts and (D) hemostasis time of various experimental groups. Data are expressed as means ± SEM ($n = 4$; $^*P < 0.05$, $^{**}P < 0.01$, and $^{***}P < 0.001$). (E) Schematic diagram of mucus penetration profiles of CaO_2 and CaO_2−Cu_2O. The reaction equation of CaO_2 and H_2O is presented in the illustration. (F) Concentrations of dissolved O_2 in CaO_2 and CaO_2−Cu_2O suspensions after incubation for 180 s. Data are expressed as means ± SEM ($n = 3$; $^*P < 0.05$, $^{**}P < 0.01$, and $^{***}P < 0.001$). (G) Mucus penetration profiles of CaO_2 and CaO_2−Cu_2O. The scale bar represents 100 μm. (H) *In vivo* imaging of the GIT showing the bio-distribution of NPs after rectal administration. Once the NP suspensions were prepared, they were rectally administered to the mice at an equal Cou amount (2 mg/kg). (I) Accumulation profiles of CaO_2@Cou and CaO_2−Cu_2O@Cou in the inflamed colon tissues. The scale bar represents 100 μm.

Please cite this article as: Xiao Bo et al., Gas-propelled nanomotors alleviate colitis through the regulation of intestinal immunoenvironment-hematopexis-microbiota circuits, Acta Pharmaceutica Sinica B, https://doi.org/10.1016/j.apsb.2024.02.008

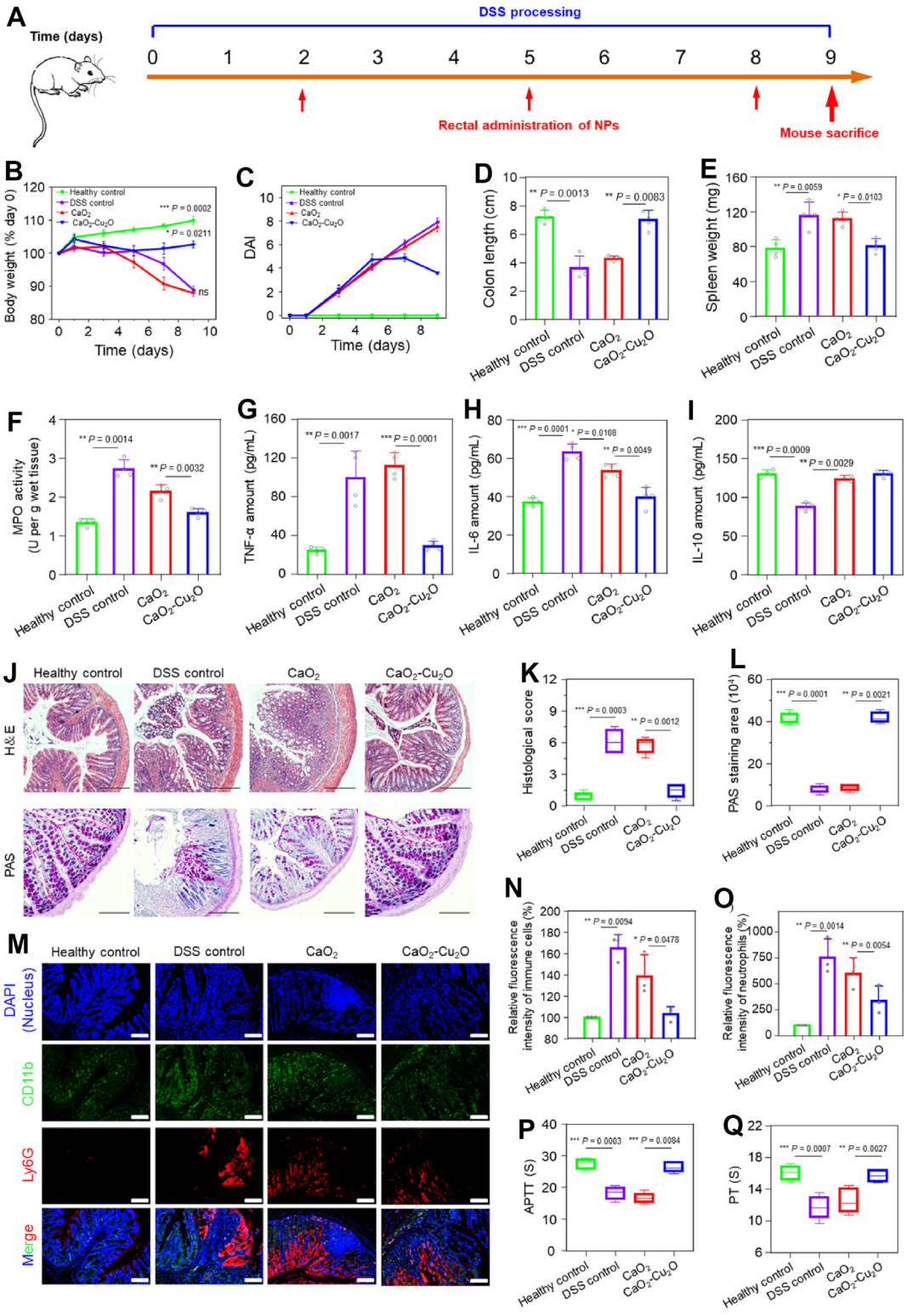

Figure 4 *In vivo* preventative effect of NPs against UC. (A) Schematic illustration of the experimental protocol. Mice were treated with DSS-contained water (3.5%, *w/v*) for 9 days and rectally administered with CaO_2 and CaO_2−Cu_2O on Days 2, 5, and 8, respectively. (B) Variations of body weights over time, normalized to the percentage of the day-zero body weight. (C) DAI values, (D) colon lengths, (E) spleen weights, and (F) MPO activities of various experimental groups. The amounts of pro-inflammatory cytokines in the serum: (G) TNF-α, (H) IL-6, and (I) IL-10. Data are expressed as means ± SEM ($n = 4$; $^*P < 0.05$, $^{**}P < 0.01$, and $^{***}P < 0.001$). (J) H&E− and PAS-stained colon tissues. The scale bar represents 20 μm. (K) Histological scores and (L) PAS staining areas of the colon tissues. (M) Images of monocyte-derived immune cells and neutrophils in the colon tissues from different experimental groups by immunofluorescent staining. The scale bar represents 50 μm. (N, O) Quantitative results of neutrophils and monocyte-derived immune cells according to the mean fluorescence intensities by CLSM analysis. Blood coagulation indexes of the serum from various experimental groups in terms of (P) APTT and (Q) PT. Data are expressed as means ± SEM ($n = 3$; $^*P < 0.05$, $^{**}P < 0.01$, and $^{***}P < 0.001$).

Please cite this article as: Xiao Bo et al., Gas-propelled nanomotors alleviate colitis through the regulation of intestinal immunoenvironment-hematopexis-microbiota circuits, Acta Pharmaceutica Sinica B, https://doi.org/10.1016/j.apsb.2024.02.008

Surprisingly, the colonic tissues from the CaO_2−Cu_2O-treated group could not identify apparent inflammatory regions, damaged epithelial barriers, and depleted goblet cells; instead, the nearly intact colonic microstructure was observed (Fig. 4J and K). DSS treatment yielded a significantly lower amount of glycomucins, and CaO_2 had no effect on mucin secretion. However, the treatment of CaO_2−Cu_2O could efficiently restore the mucin amount to the healthy colon level (Fig. 4J and L). The immunofluorescence staining results revealed that significantly increased numbers of infiltrating mononuclear phagocytes ($CD11b^+$) and neutrophils ($Ly6G^+$), as well as the moderate/severe disruption of colonic tissues, were observed in the colonic tissues from the CaO_2-treated group (Fig. 4M−O). On the contrary, mice receiving the treatment of CaO_2−Cu_2O presented much fewer $CD11b^+$ or $Ly6G^+$ cells, suggesting that this nanomotor could mitigate the infiltration of mononuclear phagocytes and neutrophils in the colon tissues. We also found that after the treatment of CaO_2−Cu_2O, the indicators of activated partial thromboplastin time (APTT) and prothrombin time (PT) were restored to the healthy control levels (Fig. 4P and Q and Supporting Information Fig. S12), which could be attributed to the coagulation effect of Ca^{2+} released from CaO_2−Cu_2O. These findings suggest that CaO_2−Cu_2O is able to mediate the recovery of the DSS-damaged coagulation system. The normalization of the typical UC symptoms gives credit to the effective anti-inflammatory, radical scavenging, and hemostatic activities of CaO_2−Cu_2O during the therapeutic procedure. Dexamethasone (DEX) is a routine drug for clinical treatment of UC. We further comparatively investigated the therapeutic outcomes of CaO_2−Cu_2O and DEX against UC. As seen in Supporting Information Fig. S13, the treatment of CaO_2−Cu_2O achieved an obviously better therapeutic efficacy against UC, in comparison with rectal DEX.

Besides its considerable therapeutic outcomes, *in vivo* biosafety is an essential indicator for the clinical translation of medical products. H&E staining results of the major organs (Supporting Information Fig. S14), organ indexes (Supporting Information Fig. S15), and hemanalysis (Supporting Information Fig. S16) demonstrated the laudable biosafety of CaO_2−Cu_2O, and this NP induced negligible damage to the five major organs (heart, liver, spleen, lung, and kidney) and obtained healthy levels of the immune-related indicators, including white blood cells (WBC), neutrophilic granulocyte (Gran), lymphocyte (lymph), and monocyte (Mon).

3.5. *Impact of CaO_2−Cu_2O on the intestinal microorganism*

The intestinal microorganism exerts diverse roles in the development and treatment response of UC, including colonic epithelial barrier function, redox equilibrium, and mucosal immune status[45]. To explore the influence of CaO_2−Cu_2O on intestinal microorganisms, 16*S* rRNA was amplified and sequenced to analyze the community distribution and diversity composition of intestinal microorganisms. Initially, operational taxonomic unit (OTU) analysis, including the Chao index (Fig. 5A), Shannon index (Fig. 5B), and Venn diagram (Supporting Information Fig. S17), suggested that the CaO_2−Cu_2O-treated group had an improved diversity of intestinal microbiota. Principal coordinates analysis (PCoA) showed that the community composition in the CaO_2−Cu_2O-treated group was close to that in the healthy control group, which was quite different from those in the DSS control group and the CaO_2-treated group (Fig. 5C). The similarity of the bacterial colony between the healthy control group and the CaO_2−Cu_2O-treated group demonstrates that CaO_2−Cu_2O is able to rebalance the intestinal microbiota. To further ensure the influence of CaO_2−Cu_2O on microbiota, the microflora compositions of all the groups were detected at the genus level (Supporting Information Fig. S18). It was found that CaO_2−Cu_2O had the ability to regulate the interaction of enteric microorganisms. Heat map, a clustering analysis method, revealed that the CaO_2−Cu_2O-treated group mainly presented the increased abundance in *Alistipes* and the decreased quantity in *Clostridium* and *Romboutsia* in contrast with the DSS control group, almost similar to those in the healthy control group (Supporting Information Fig. S19).

We detected a series of bacterium abundance to evaluate the capacity of CaO_2−Cu_2O to regulate the GIT ecosystem. Short-chain fatty acids (SCFA) are essential for maintaining the balance of intestinal flora and the viability of colonic epithelial cells[46]. *Odoribacter* and *Faecalibaculum*, as beneficial symbiotic bacteria producing SCFA, showed much higher abundances in the healthy control group and the CaO_2−Cu_2O-treated group when compared with the DSS control group, particularly for *Odoribacter* (Fig. 5D and E). *Roseburia* displays an anti-inflammatory property by inhibiting the activation of macrophages in UC *via* propagating the butyrate metabolic pathway, which also restores the structural integrity of the colon. Fig. 5F showed that rectal administration of CaO_2−Cu_2O induced a slightly increased abundance of *Roseburia*. Meanwhile, for beneficial bacteria (*e.g.*, *Phascolarctobacterium*, *Bifidobacterium*, and *Alistipes*) in protecting the intestinal barrier, their abundances in the healthy control group and the CaO_2−Cu_2O-treated group were significantly higher than those in the DSS control group and the CaO_2-treated group (Fig. 5G−I). In addition to up-regulating the abundance of beneficial bacteria, CaO_2−Cu_2O could markedly down-regulate the proportions of harmful bacteria. As shown in Fig. 5J−L, the levels of pathogenic bacteria, including *Escherichia coli*, *Prevotellaceae*, and *Helicobacter*, were largely decreased in the CaO_2−Cu_2O-treated group compared with those in the DSS control group and the CaO_2-treated group. A sequence of results suggests that CaO_2−Cu_2O has the ability to regulate the GIT ecosystem by upgrading microbiome richness and diversity, promoting beneficial bacteria proportions, restricting the proliferation of pathogenic bacteria, and eventually maintaining microbiota balance.

3.6. *Preventive mechanism of CaO_2−Cu_2O against UC*

Although CaO_2−Cu_2O showed good performance in regulating immune-hematopoiesis-microbiota, we further explored its underlying preventive mechanism using bioinformatics analysis. The volcano plots quantitatively displayed the up-regulation, down-regulation, and insignificance of genes between the two groups (Supporting Information Fig. S20). There were 723 up-regulated differentially expressed genes (DEGs) and 182 down-regulated DEGs in the CaO_2−Cu_2O-treated group against the healthy control group. However, compared with the DSS control group, 831 DEGs were significantly up-regulated, and 213 DEGs were down-regulated in the CaO_2−Cu_2O-treated group. The Venn diagram and the upset plot implied that 14276 genes were co-expressed in

Please cite this article as: Xiao Bo et al., Gas-propelled nanomotors alleviate colitis through the regulation of intestinal immunoenvironment-hematopexis-microbiota circuits, Acta Pharmaceutica Sinica B, https://doi.org/10.1016/j.apsb.2024.02.008

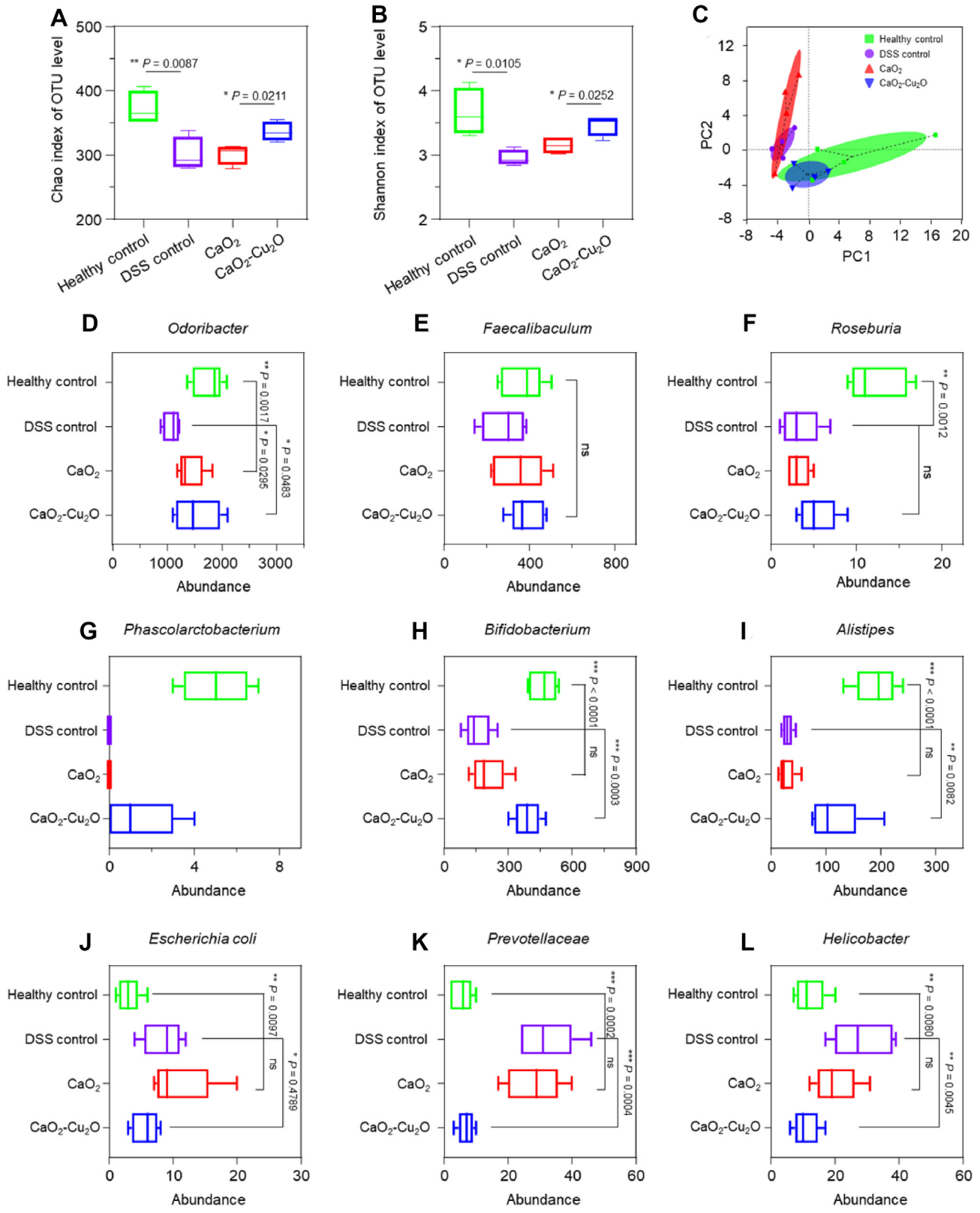

Figure 5 Analysis of intestinal microorganisms from various experimental groups. (A) Chao and (B) Shannon indexes on OUT levels. (C) PCoA analysis of the bacterial colony. The abundance of (D) *Odoribacter*, (E) *Faecalibaculum*, (F) *Roseburia*, (G) *Phascolarctobacterium*, (H) *Bifidobacterium*, (I) *Alistipes*, (J) *Escherichia coli*, (K) *Prevotellaceae*, and (L) *Helicobacter* in the feces from various experimental groups. Data are expressed as means ± SEM ($n = 4$; $^{*}P < 0.05$, $^{**}P < 0.01$, and $^{***}P < 0.001$).

Please cite this article as: Xiao Bo et al., Gas-propelled nanomotors alleviate colitis through the regulation of intestinal immunoenvironment-hematopexis-microbiota circuits, Acta Pharmaceutica Sinica B, https://doi.org/10.1016/j.apsb.2024.02.008

all the groups, and there were also a substantial number of DEGs (Supporting Information Fig. S21). We further found that the gene expression profile of the CaO_2−Cu_2O-treated group was closely related to the healthy control group. Next, gene set enrichment analysis was applied to interpret CaO_2−Cu_2O-associated metabolic and signaling pathways. The enriched GO terms implied that the effective remission of CaO_2−Cu_2O against UC was associated with abundant immune or anti-oxidative signaling pathways, including B and T cell receptor-mediated signaling pathway, activation of natural killer cells, lymphocyte migration, ROS metabolic process, $O_2^{\bullet-}$ generation, and NO biosynthetic process (Fig. 6A).

To contextualize the specific genes associated with identified metabolic and signaling pathways, we applied hierarchical clustering analysis and generated the heat map to visualize the gene semantic similarities and differences among 4 experimental groups. As seen in Fig. 6B, many representative pro-inflammatory and immune genes (*e.g., Tnf-α, Il-6, Il-1β, Cd4,* and *Cd8*) were remarkably down-regulated in the CaO_2−Cu_2O-treated group. Meanwhile, up-regulated chemokine genes (*e.g.*, *Ccl2*, *Ccl3*, *Ccl4*, *Ccl5*, *Cxcr2*, and *Cxcl10*) in recruiting various immune cells and regulating mucosal inflammation in DSS-induced UC were significantly restrained in the CaO_2−Cu_2O-treated group. The results suggest that three dosages of CaO_2−Cu_2O reduce the pro-inflammatory cytokines and chemokines.

To further elucidate the underlying biological mechanisms of CaO_2−Cu_2O-associated DEGs, protein−protein interaction (PPI) networks were constructed using the Majorbio I-Sanger software. The top 7 hub genes (*Tnf-α*, *Il-1β*, *Cd4*, *Itgb2*, mmol/L*p-9*, *Ccl-5*, and *Syk*) were identified based on the degree values (>10) (Supporting Information Fig. S22). Among the encoded proteins, TNF-α, IL-1β, and CD4 played a pivotal role in the immune modulating function of the healthy tissue, with a high consistency to the previous studies[47]. Interestingly, *Tnf-α* and *Il-1β* were also identified as the hub nodes in the CaO_2−Cu_2O-treated group, confirming the immune regulatory functions of CaO_2−Cu_2O (Supporting Information Fig. S23). Moreover, we found that other identified hub nodes in the CaO_2−Cu_2O-treated group were *nitric oxide synthase 1* (*Nos1*), *Cd163*, and *haptoglobin* (*Hp*) (Supporting Information Fig. S24A), which were crucial in the progression of UC. NOS1 serves as a primary factor in the synthetic process of nitric oxide and regulating the immune responses of the mucosa[48]. HP is one of the plasma proteins, which captures hemoglobin (Hb) in hemolysis and acts as an anti-oxidative molecule and an immunomodulator during hemolysis[49]. CD163, an Hb-HP scavenger receptor, is a macrophage-specific protein that can protect inflammatory tissues from free Hb-mediated oxidative damage[50,51]. The synergistic function of HP and CD163 contributes to promoting the coagulation effect and the ROS scavenging of macrophages, avoiding blood loss and oxidative damage.

The expression profiles of 5 hub genes (Fig. 6C) and closely related genes (Fig. 6D and E) in the colons were quantitatively displayed. CD163 is considered a biomarker that is highly expressed in macrophages exhibiting an anti-inflammatory feature. Significantly increased CD163 expression was detected in the CaO_2−Cu_2O-treated mice. These hub genes perform a vital function in the therapeutic mechanism of CaO_2−Cu_2O in UC. Treatment of CaO_2−Cu_2O successfully lowered the DSS-elevated level of plasma HP, suggesting the protective effect of CaO_2−Cu_2O in ameliorating colonic inflammation-induced oxidative stress. A much higher level of NOS suggests an imbalanced M1/M2 ratio in the DSS-induced UC mouse model[52]. The therapeutic effect of CaO_2−Cu_2O against UC might be mediated by promoting the polarization to M2 macrophages and equilibrating the M1/M2 ratio relative to the healthy level. The construction of the PPI network of immune factors, including immune-stimulatory factors, immune-inhibitory factors, chemokines, and receptors around the hub nodes of CaO_2−Cu_2O, could comprehend the immune regulatory functions of CaO_2−Cu_2O (Fig. S24B).

The transcriptome results illustrated that the effective treatment of CaO_2−Cu_2O in UC was closely connected with regulating inflammatory reactions and preventing tissue damage *via* the down-regulation of TNF-α, IL-1β, and IFN-γ, as well as restraining the oxidative responses. At the same time, the improved coagulation functions of CaO_2−Cu_2O depended upon the regulation of *Nos*, *Hp*, and *Cd163* (Fig. 6F). In summary, the four primary synergetic links contribute to the therapeutic outcomes of CaO_2−Cu_2O against UC.

3.7. *In vivo therapeutic effect of CaO_2−Cu_2O against UC*

To further confirm the UC therapeutic effect of CaO_2−Cu_2O, mice were processed by clyster administration following the treatment protocol in Fig. 7A. The body weights of all DSS-involved groups exhibited an upward tendency from the fifth day. In particular, the CaO_2−Cu_2O-treated group showed a rapid weight gain when compared with other DSS-involved groups (Fig. 7B). DAI values presented an accelerated decline after the rectal administration of CaO_2−Cu_2O, demonstrating that this NP efficiently restricted the progression of UC (Fig. 7C). Simultaneously, the CaO_2−Cu_2O-treated group displayed restored colon length (Fig. 7D and Supporting Information Fig. S25) and spleen weight (Fig. 7E). Nevertheless, multiple indicators were measured to assess the therapeutic outcomes of CaO_2−Cu_2O, such as MPO, pro-inflammatory cytokines (*e.g.,* TNF-α and IL-6), and anti-inflammatory cytokines (*e.g.,* IL-10). As revealed in Fig. 7F−I, CaO_2−Cu_2O significantly inhibited the amounts of MPO produced by neutrophils and the secreted levels of pro-inflammatory cytokines while up-regulating IL-10. These results reflect that CaO_2−Cu_2O not only retards the development of UC but also possesses an undeniably therapeutic effect against UC.

H&E and PAS staining results revealed immune cell infiltration and structural damage in the colonic tissues from the DSS control group and the CaO_2-treated group. There were no apparent lesions and intact crypt structures in the CaO_2−Cu_2O-treated group (Fig. 7J). Semi-quantitatively, the histological scores revealed that the treatment of CaO_2−Cu_2O nearly restored the colonic phenotype to a healthy appearance (Fig. 7K). As seen in Supporting Information Fig. S26, there was no significant difference in organ indexes among all mouse groups, illustrating the excellent biosafety of CaO_2−Cu_2O. In the context of PAS staining, no significant difference was observed in the colonic mucosa between the healthy control group and the CaO_2−Cu_2O-treated group. Their mucus amounts were over 2.0-fold higher than those in the DSS control group as well as the CaO_2-treated groups (Fig. 7L). Meanwhile, immunofluorescence staining results showed that CaO_2−Cu_2O treatment led to the lowest $CD11b^+$ and $Ly6G^+$ cells among all mouse groups, effectively reducing the infiltration of neutrophils and immune cells in the colonic tissues (Fig. 7M−O). Moreover, the anus photographs were recorded to observe the

Please cite this article as: Xiao Bo et al., Gas-propelled nanomotors alleviate colitis through the regulation of intestinal immunoenvironment-hematopexis-microbiota circuits, Acta Pharmaceutica Sinica B, https://doi.org/10.1016/j.apsb.2024.02.008

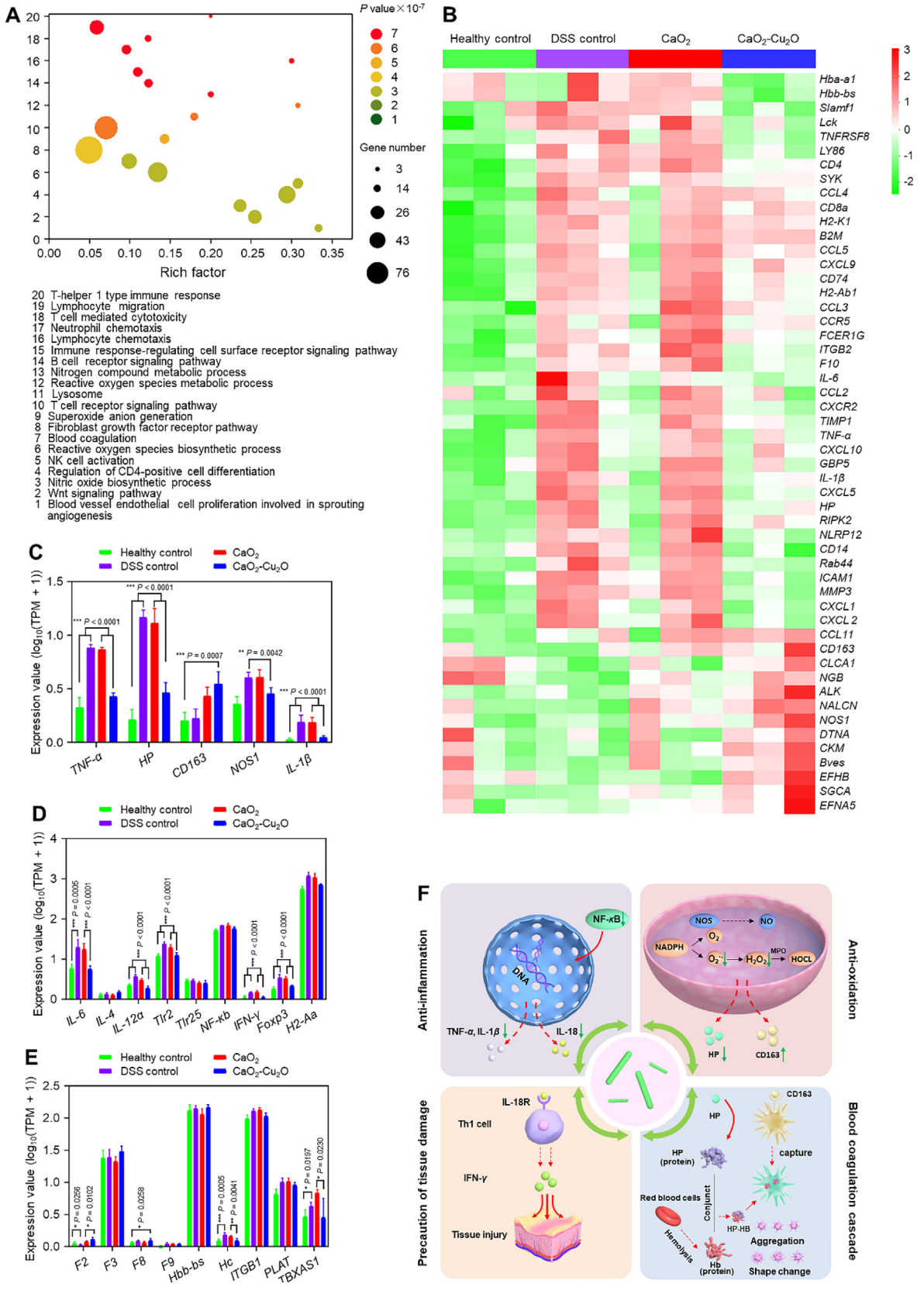

Figure 6 Gene expression profiles of the colon tissues from various experimental groups at the transcriptome level. (A) GO enrichment and (B) hierarchical clustering analysis. Expression of (C) Hub genes and (D, E) closely related genes in the colon tissues from various experimental groups. (F) Schematic diagram of the therapeutic mechanism of CaO_2−Cu_2O against UC. Data are expressed as means ± SEM ($n = 3$; $^*P < 0.05$, $^{**}P < 0.01$, and $^{***}P < 0.001$).

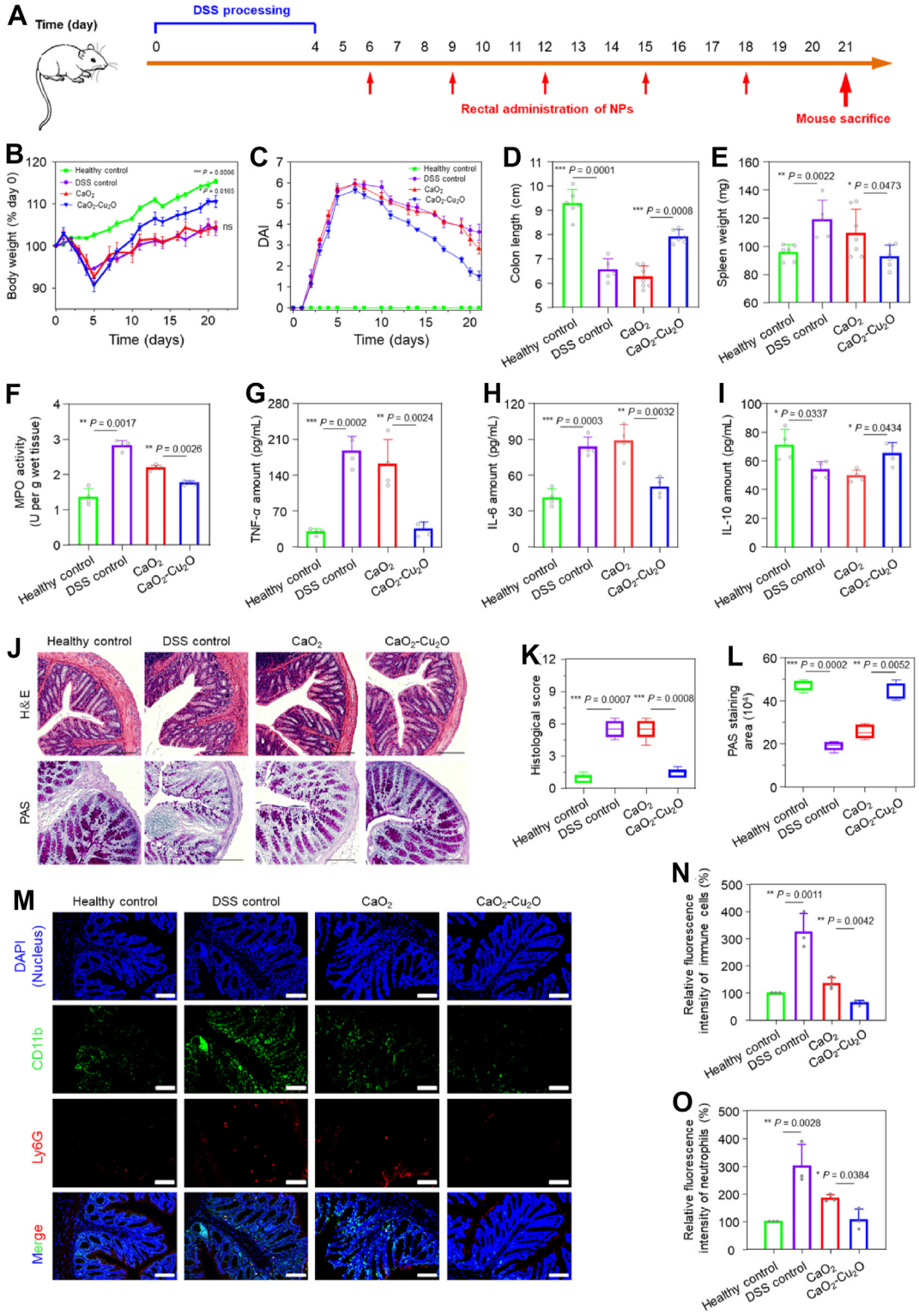

Figure 7 *In vivo* therapeutic outcomes of various NPs against UC. (A) Schematic illustration of the experimental protocol. Mice were treated with DSS-contained water (4.5%, *w/v*) for 5 days. After that, mice were treated with CaO_2 and CaO_2−Cu_2O every three days *via* rectal administration. (B) Variations of body weights over time, normalized to the percentage of the day-zero body weight. (C) DAI values, (D) colon lengths, (E) spleen weights, and (F) MPO activities of various experimental groups. Data are expressed as means ± SEM ($n = 5$−7; $^*P < 0.05$, $^{**}P < 0.01$, and $^{***}P < 0.001$). The amounts of pro-inflammatory cytokines in the serum: (G) TNF-α, (H) IL-6, and (I) IL-10. Data are expressed as means ± SEM ($n = 4$; $^*P < 0.05$, $^{**}P < 0.01$, and $^{***}P < 0.001$). (J) H&E-stained and PAS-stained colon tissues. The scale bar represents 20 μm. (K) Histological scores and (L) PAS staining areas of the colon tissues. (M) Images of monocyte-derived immune cells and neutrophils in the colon tissues from different experimental groups by immunofluorescent staining. The scale bar represents 50 μm. Quantitative results of (N) monocyte-derived immune cells and (O) neutrophils according to the mean fluorescence intensities by CLSM analysis. Data are expressed as means ± SEM ($n = 3$; $^*P < 0.05$, $^{**}P < 0.01$, and $^{***}P < 0.001$).

Please cite this article as: Xiao Bo et al., Gas-propelled nanomotors alleviate colitis through the regulation of intestinal immunoenvironment-hematopexis-microbiota circuits, Acta Pharmaceutica Sinica B, https://doi.org/10.1016/j.apsb.2024.02.008

hematochezia of mice. Supporting Information Fig. S27 indicated that the CaO_2−Cu_2O-treated group presented a more rapid recovery effect of hematochezia than the DSS control group and the CaO_2-treated group.

The H&E staining and hemanalysis were again used to evaluate the biosafety of CaO_2−Cu_2O. The negligible lesions of the main organs verified their favorable biocompatibility (Supporting Information Fig. S28). The detected indicators of the CaO_2−Cu_2O-treated group showed an extreme similarity with the healthy control group on hemanalysis results, affirming its good biological safety (Supporting Information Fig. S29). The superior therapeutic outcomes and the biosafety of CaO_2−Cu_2O demonstrate their promising potential to defeat UC.

4. Conclusions

We proposed a versatile therapeutic system, a rectally administered CaO_2−Cu_2O nanomotor, which accumulated in the colitis mucosa following gas-impulsively penetrating through the mucus layer and disrupted epithelial barrier. Rectal administration into the colon lumen and gas-propelled mucus penetration cooperatively reduced the systematic exposure and improved the accumulation of CaO_2−Cu_2O in the colonic mucosa. Multiple strategies of anti-oxidation, anti-inflammation, macrophage polarization, and regulation of intestinal flora allowed CaO_2−Cu_2O to create a prominently alleviative and therapeutic effect against ulcerative colitis (UC). The desirable therapeutic outcomes were tied firmly to the regulation of hub genes (*Tnf-α*, *Il-1β*, *Il-6*, *Nos1*, *Cd163*, and *Hp*). Collectively, our versatile nanomotor provides an efficient and safe therapeutic platform for managing UC, which shows promising potential for biomedical translation.

Acknowledgments

This study was supported by the National Natural Science Foundation of China (82072060, 82360110, and 22008201), the Fundamental Research Funds for the Central Universities (SWU-XDPY22006, China), the Venture & Innovation Support Program for Chongqing Overseas Returnees (2205012980212766, China), the Distinguished Young Scholars of Chongqing (2022NSCQ-JQX5279, China), and the Science and Technology Department of Jiangxi Province (20212BDH81019 and 20224BAB206073, China).

Author contributions

Bo Xiao, Yuqi Liang, and Zhenghua Zhu designed experiments, supervised the project, and wrote the draft of manuscript. Bo Xiao, Yuqi Liang, Ga Liu, Lingshuang Wang, Libin Qiu, and Haiting Xu performed the experiments. Bo Xiao, Yuqi Liang, Ga Liu, Zhan Zhang, Sean Carr, Xiaoxiao Shi, Rui L. Reis, Subhas C. Kundu, and Zhenghua Zhu edited and revised the manuscript. All authors have given approval to the final version of the manuscript.

Conflicts of interest

The authors have no conflicts of interest to declare.

Appendix A. Supporting information

Supporting data to this article can be found online at https://doi.org/10.1016/j.apsb.2024.02.008.

References

1. Ungaro R, Mehandru S, Allen PB, Peyrin-Biroulet L, Colombel JF. Ulcerative colitis. *Lancet* 2017;**389**:1756−70.
2. Uzzan M, Martin JC, Mesin L, Livanos AE, Castro-Dopico T, Huang R, et al. Ulcerative colitis is characterized by a plasmablast-skewed humoral response associated with disease activity. *Nat Med* 2022;**28**:766−79.
3. Doherty G, Katsanos KH, Burisch J, Allez M, Papamichael K, Stallmach A, et al. European crohn's and colitis organisation topical review on treatment withdrawal 'exit strategies' in inflammatory bowel disease. *J Crohns Colitis* 2018;**12**:17−31.
4. Du L, Ha C. Epidemiology and pathsssogenesis of ulcerative colitis. *Gastroenterol Clin* 2020;**49**:643−54.
5. Shanahan F. Pathogenesis of ulcerative colitis. *Lancet* 1993;**342**:407−11.
6. Vande Casteele N, Leighton JA, Pasha SF, Cusimano F, Mookhoek A, Hagen CE, et al. Utilizing deep learning to analyze whole slide images of colonic biopsies for associations between eosinophil density and clinicopathologic features in active ulcerative colitis. *Inflamm Bowel Dis* 2022;**28**:539−46.
7. Mills RH, Dulai PS, Vazquez-Baeza Y, Sauceda C, Daniel N, Gerner RR, et al. Multi-omics analyses of the ulcerative colitis gut microbiome link *Bacteroides vulgatus* proteases with disease severity. *Nat Microbiol* 2022;**7**:262−76.
8. Chassaing B, Koren O, Goodrich JK, Poole AC, Srinivasan S, Ley RE, et al. Dietary emulsifiers impact the mouse gut microbiota promoting colitis and metabolic syndrome. *Nature* 2015;**519**:92−6.
9. Pittayanon R, Lau JT, Leontiadis GI, Tse F, Yuan Y, Surette M, et al. Differences in gut microbiota in patients with vs without inflammatory bowel diseases: a systematic review. *Gastroenterology* 2020;**158**:930−46.
10. Xiao B, Zhang Z, Viennois E, Kang Y, Zhang M, Han MK, et al. Combination therapy for ulcerative colitis: orally yargeted nanoparticles prevent mucosal damage and relieve inflammation. *Theranostics* 2016;**6**:2250−66.
11. Kotla NG, Rana S, Sivaraman G, Sunnapu O, Vemula PK, Pandit A, et al. Bioresponsive drug delivery systems in intestinal inflammation: state-of-the-art and future perspectives. *Adv Drug Deliv Rev* 2019;**146**:248−66.
12. Schaap FG, Trauner M, Jansen PL. Bile acid receptors as targets for drug development. *Nat Rev Gastroenterol* 2014;**11**:55.
13. Zu M, Ma Y, Cannup B, Xie D, Jung Y, Zhang J, et al. Oral delivery of natural active small molecules by polymeric nanoparticles for the treatment of inflammatory bowel diseases. *Adv Drug Deliv Rev* 2021;**176**:113887.
14. Liu M, Zhang J, Shan W, Huang Y. Developments of mucus penetrating nanoparticles. *Asian J Pharm Sci* 2015;**10**:275−82.
15. Liu Y, Jiang Z, Hou X, Xie X, Shi J, Shen J, et al. Functional lipid polymeric nanoparticles for oral drug delivery: rapid mucus penetration and improved cell entry and cellular transport. *Nanomedicine* 2019;**21**:102075.
16. Wei Y, Li X, Lin J, Zhou Y, Yang J, Hou M, et al. Oral delivery of siRNA using fluorinated, small-sized nanocapsules toward anti-inflammation treatment. *Adv Mater* 2022;**35**:e2206821.
17. Yang M, Lai SK, Wang YY, Zhong W, Happe C, Zhang M, et al. Biodegradable nanoparticles composed entirely of safe materials that rapidly penetrate human mucus. *Angew Chem* 2011;**50**:2597−600.
18. Gao C, Wang Y, Ye Z, Lin Z, Ma X, He Q. Biomedical micro-/nanomotors: from overcoming biological barriers to *in vivo* imaging. *Adv Mater* 2021;**33**:e2000512.
19. Chen W, Jiang R, Sun X, Chen S, Liu X, Fu M, et al. Self-fueled janus nanomotors as active drug carriers for propulsion behavior-reinforced permeability and accumulation at the tumor site. *Chem Mater* 2022;**34**:7543−52.
20. Ortiz-Rivera I, Mathesh M, Wilson DA. A supramolecular approach to nanoscale motion: polymersome-based self-propelled nanomotors. *Acc Chem Res* 2018;**51**:1891−900.

21. Wang H, Chen X, Qi Y, Wang C, Huang L, Wang R, et al. Self-propelled nanomotors with alloyed engine for emergency rescue of traumatic brain injury. *Adv Mater* 2022;**34**:e2206779.
22. Kong H, Chu Q, Fang C, Cao G, Han G, Li X. Cu-ferrocene-functionalized CaO(2) nanoparticles to enable tumor-specific synergistic therapy with GSH depletion and calcium overload. *Adv Sci* 2021;**8**:e2100241.
23. Baylis JR, Yeon JH, Thomson MH, Kazerooni A, Wang X, John AE St, et al. Self-propelled particles that transport cargo through flowing blood and halt hemorrhage. *Sci Adv* 2015;**1**:e1500379.
24. Cao W, Liu Y, Ran P, He J, Xie S, Weng J, et al. Ultrasound-propelled janus rod-shaped micromotors for site-specific sonodynamic thrombolysis. *ACS Appl Mater Interfaces* 2021;**13**:58411−21.
25. Liu T, Xiao B, Xiang F, Tan J, Chen Z, Zhang X, et al. Ultrasmall copper-based nanoparticles for reactive oxygen species scavenging and alleviation of inflammation related diseases. *Nat Commun* 2020;**11**:2788.
26. Kornbluth A, Sachar DB. Ulcerative colitis practice guidelines in adults: American college of gastroenterology, practice parameters committee. *Am J Gastroenterol* 2010;**105**:501−23.
27. Harris MS, Lichtenstein GR. Review article: delivery and efficacy of topical 5-aminosalicylic acid (mesalazine) therapy in the treatment of ulcerative colitis. *Aliment Pharmacol Ther* 2011;**33**:996−1009.
28. Yang S, Lian G. ROS and diseases: role in metabolism and energy supply. *Mol Cell Biochem* 2020;**467**:1−12.
29. Wu C, Xu D, Ge M, Luo J, Chen L, Chen Z, et al. Blocking glutathione regeneration: inorganic NADPH oxidase nanozyme catalyst potentiates tumoral ferroptosis. *Nano Today* 2022;**46**:101574.
30. Pelaz B, Alexiou C, Alvarez-Puebla RA, Alves F, Andrews AM, Ashraf S, et al. Diverse applications of nanomedicine. *ACS Nano* 2017;**11**:2313−81.
31. Bai S, Lan Y, Fu S, Cheng H, Lu Z, Liu G. Connecting calcium-based nanomaterials and cancer: from diagnosis to therapy. *Nano-Micro Lett* 2022;**14**:145.
32. Na YR, Stakenborg M, Seok SH, Matteoli G. Macrophages in intestinal inflammation and resolution: a potential therapeutic target in IBD. *Nat Rev Gastroenterol* 2019;**16**:531−43.
33. Ma Y, Duan L, Sun J, Gou S, Chen F, Liang Y, et al. Oral nanotherapeutics based on *Antheraea pernyi* silk fibroin for synergistic treatment of ulcerative colitis. *Biomaterials* 2022;**282**:121410.
34. Lin R, Deng C, Li X, Liu Y, Zhang M, Qin C, et al. Copper-incorporated bioactive glass-ceramics inducing anti-inflammatory phenotype and regeneration of cartilage/bone interface. *Theranostics* 2019;**9**:6300−13.
35. Zarkovic N. Roles and functions of ROS and RNS in cellular physiology and pathology. *Cells* 2020;**9**:767.
36. Kaenkumchorn T, Wahbeh G. Ulcerative colitis: making the diagnosis. *Gastroenterol Clin* 2020;**49**:655−69.
37. Wu Z, Zeng H, Zhang L, Pu Y, Li S, Yuan Y, et al. Patchouli alcohol: a natural sesquiterpene against both inflammation and intestinal barrier damage of ulcerative colitis. *Inflammation* 2020;**43**:1423−35.
38. Hong L, Chen G, Cai Z, Liu H, Zhang C, Wang F, et al. Balancing microthrombosis and inflammation *via* injectable protein hydrogel for inflammatory bowel disease. *Adv Sci* 2022;**9**:e2200281.
39. Cao Y, Liu S, Ma Y, Ma L, Zu M, Sun J, et al. Oral nanomotor-enabled mucus traverse and tumor penetration for targeted chemo-sono-immunotherapy against colon cancer. *Small* 2022;**18**:e2203466.
40. Gao W, de Avila BE, Zhang L, Wang J. Targeting and isolation of cancer cells using micro/nanomotors. *Adv Drug Deliv Rev* 2018;**125**:94−101.
41. Zhou X, Liu Y, Huang Y, Ma Y, Lv J, Xiao B. Mucus-penetrating polymeric nanoparticles for oral delivery of curcumin to inflamed colon tissue. *J Drug Deliv Sci Technol* 2019;**52**:157−64.
42. Cubillos-Ruiz A, Guo T, Sokolovska A, Miller PF, Collins JJ, Lu TK, et al. Engineering living therapeutics with synthetic biology. *Nat Rev Drug Discov* 2021;**20**:941−60.
43. Deshaies RJ. Multispecific drugs herald a new era of biopharmaceutical innovation. *Nature* 2020;**580**:329−38.
44. Yan YX, Shao MJ, Qi Q, Xu YS, Yang XQ, Zhu FH, et al. Artemisinin analogue SM934 ameliorates DSS-induced mouse ulcerative colitis *via* suppressing neutrophils and macrophages. *Acta Pharmacol Sin* 2018;**39**:1633−44.
45. Xu J, Xu J, Shi T, Zhang Y, Chen F, Yang C, et al. Probiotic-inspired nanomedicine restores intestinal homeostasis in colitis by regulating redox balance, immune responses, and the gut microbiome. *Adv Mater* 2023;**35**:e2207890.
46. Lee JY, Tsolis RM, Bäumler AJ. The microbiome and gut homeostasis. *Science* 2022;**377**:eabp9960.
47. Xue G, Hua L, Zhou N, Li J. Characteristics of immune cell infiltration and associated diagnostic biomarkers in ulcerative colitis: results from bioinformatics analysis. *Bioengineered* 2021;**12**:252−65.
48. Dong X, Fu Q, Liu S, Gao C, Su B, Tan F, et al. The expression signatures of neuronal nitric oxide synthase (NOS1) in turbot (*Scophthalmus maximus* L.) mucosal surfaces against bacterial challenge. *Fish Shellfish Immunol* 2016;**59**:406−13.
49. Vanuytsel T, Vermeire S, Cleynen I. The role of haptoglobin and its related protein, Zonulin, in inflammatory bowel disease. *Tissue Barriers* 2013;**1**:e27321.
50. Etzerodt A, Moestrup SK. CD163 and inflammation: biological, diagnostic, and therapeutic aspects. *Antioxidants Redox Signal* 2013;**18**:2352−63.
51. Nielsen MC, Hvidbjerg Gantzel R, Clària J, Trebicka J, Møller HJ, Grønbæk H. Macrophage activation markers, CD163 and CD206, in acute-on-chronic liver failure. *Cells* 2020;**9**:1175.
52. Zhu W, Yu J, Nie Y, Shi X, Liu Y, Li F, et al. Disequilibrium of M1 and M2 macrophages correlates with the development of experimental inflammatory bowel diseases. *Immunol Invest* 2014;**43**:638−52.

Please cite this article as: Xiao Bo et al., Gas-propelled nanomotors alleviate colitis through the regulation of intestinal immunoenvironment-hematopexis-microbiota circuits, Acta Pharmaceutica Sinica B, https://doi.org/10.1016/j.apsb.2024.02.008